

RSC Advances



This is an *Accepted Manuscript*, which has been through the Royal Society of Chemistry peer review process and has been accepted for publication.

Accepted Manuscripts are published online shortly after acceptance, before technical editing, formatting and proof reading. Using this free service, authors can make their results available to the community, in citable form, before we publish the edited article. This *Accepted Manuscript* will be replaced by the edited, formatted and paginated article as soon as this is available.

You can find more information about *Accepted Manuscripts* in the [Information for Authors](#).

Please note that technical editing may introduce minor changes to the text and/or graphics, which may alter content. The journal's standard [Terms & Conditions](#) and the [Ethical guidelines](#) still apply. In no event shall the Royal Society of Chemistry be held responsible for any errors or omissions in this *Accepted Manuscript* or any consequences arising from the use of any information it contains.

ARTICLE

Synthesis and Electrochemical Properties of Reduced Graphene Oxide / Manganese oxide / Polyaniline Composites

Cite this: DOI: 10.1039/x0xx00000x

Received 00th January 2012,
Accepted 00th January 2012

DOI: 10.1039/x0xx00000x

www.rsc.org/

Wenjing Huang,^a Tianyuan Yao,^a Qingli Hao,^{*a} Wenjuan Wang,^a Xifeng Xia,^a Xin Wang^a

Graphene oxide/manganese oxide/polyaniline composite (GOM) was synthesized via one-step method at room temperature, and its reduced graphene oxide/manganese oxide / polyaniline (RGOM) composites were prepared under different reaction conditions. The relationships of synthesis approach, structure and electrochemical properties of the manganese oxide ternary composites were systematically investigated. The reaction temperature and the basic concentration played important roles in the reduction process. The possible reaction mechanisms of the ternary composites were proposed. The results show that high temperature under hydrothermal condition can lead to the higher crystalline degree, and promote the formation of its fiber-like nanostructure of the composites. Meanwhile, the higher concentration of NaOH promotes the reduction of MnO₂ to other manganese oxides with a lower valence. The electrochemical characterization shows that, among those composites, the specific capacity of RGOM5 with a rough and sheathed nanostructure, obtained using 8 M NaOH at 120 °C via a hydrothermal method, can reach 344 F·g⁻¹ at a scan rate of 1 mV·s⁻¹, and the capacitive retention proportion remains nearly 100% after 6000 cycles, which presents a promising future for RGOM composites acting as low cost energy storage materials.

1. Introduction

Electrochemical capacitors (ECs), also known as ultracapacitors or supercapacitors, have attracted increasing attention due to their good reversibility, high power density and long cycle life.^{1,2} ECs can be categorized into two types: electric double-layer capacitors (EDLCs) and pseudocapacitors (redox supercapacitors).³ Carbon materials, such as graphene,^{4,5} activated carbon,⁶ carbon nanotubes (CNTs),⁷

and carbon fibers,^{8,9} are used as electrode materials for EDLCs with long cyclic stability. Electrode materials for pseudo-capacitors are typically conducting polymers^{10,11} and transition metal oxides¹²⁻¹⁴ (such as manganese oxide) showing high specific capacitance. However, these electrode materials for pseudo-capacitors show poor cyclic stability. The combination of such

ARTICLE

pseudocapacitance materials with carbon materials has become acceptable strategy for improving the stability and other electrochemical performances.¹⁵ For instance, Lake *et al.* prepared the strong interaction of GO with MnO₂ nanostructures to enhance the energy density,¹⁶ Cheng *et al.* reported a freestanding and flexible graphene / polyaniline (PANI) composite paper by an in situ anodic electropolymerization of polyaniline film on graphene paper with a specific capacitance (*C*) of 233 F·g⁻¹.¹⁷

Recently, considerable attention has been paid toward manganese oxide owing to its low cost, high theoretical capacitance, low toxicity, and natural abundance.¹⁸ Moreover, the electrochemical properties are closely related to its chemical composition, oxidation states and crystallographic structure.^{19, 20} Devaraj *et al.* reported the specific capacitance (*C*) of MnO₂ depended strongly on the crystallographic structure (namely α , β , γ , δ and λ structures) and its *C* decreased in the following order: $\alpha \cong \delta > \gamma > \lambda > \beta$.²¹ Nathan *et al.* prepared the Mn₂O₃ nanospheres by a sonochemical / solvothermal route with a *C* of 100 F·g⁻¹ at 5 mV·s⁻¹.²² Moreover, the preparation methods can also influence the electrochemical performance of the manganese oxide with the same oxidation state and crystalline form,²³ because of the different structures and properties under different process conditions.

However, the low conductivity of manganese oxide limits its application as a single electrode material. Previous studies have been

reported that the conductive additives such as carbon materials^{15, 24, 25} and conducting polymer^{26, 27} are incorporated into the manganese oxide film to enhance the electrical conductivity of the electrodes. Chou *et al.* recently synthesized MnO₂ nanowire / carbon nanotube composites with *C* of 167.5 F·g⁻¹ at a current density of 77 mA·g⁻¹.²⁸ Meng *et al.* fabricated MnO₂ / polyaniline composites by one-step interfacial polymerization, and the *C* of the composites was 207 F·g⁻¹ at 50 mV·s⁻¹.²⁹ Guo *et al.* succeeded in designing a hierarchically nanostructured composite of birnessite-type manganese oxide / poly-(3, 4-ethylenedioxythiophene) / graphene, and the composite can produce a reversible capacity more than ten times that of plain MnO₂-based devices.³⁰ Wang *et al.* synthesized sulfonated graphene / MnO₂ / polyaniline composites via a dilute in-situ polymerization method with *C* of 276 F·g⁻¹ at 1 A·g⁻¹.³¹ The combination of such conductive components and manganese oxide can effectively improve the electrochemical performance of the electrodes. However, other composites containing manganese oxide with different valences have been seldom reported for supercapacitors.

Herein, we prepared various ternary nanocomposites containing PANI, manganese oxides with different valences and reduced graphene oxide (RGO) via different reduction approaches, by using aniline, KMnO₄ and graphene oxide (GO) as the precursors of three components. The two-step synthetic processes are illustrated in Scheme 1.

ARTICLE



Scheme 1 Schematic illustration of two-step synthesis of GOM and RGOM.

To the best of our knowledge, the relationship of synthesis approach, structure and electrochemical properties of manganese oxide ternary composites with RGO and PANI has been rarely studied systematically by now. In this article, the effects of various experimental parameters on the chemical structures, crystalline forms, morphology and the electrochemical performance of the as-prepared ternary nanocomposites have been systematically investigated. The fiber-like composite with rough nanostructure exhibits better electrochemical stability and supercapacitive performance than those with other structures. The composite exhibits the better supercapacitive performance than those with other structures, and the excellent cycling stability with the capacitive retention proportion of nearly 100% after 6000 cycles.

2. Experimental

2.1. Chemical Reagents

KMnO_4 , NaOH and ethanol were analytical reagent grade. Aniline was further distilled under reduced pressure. Millipore water from a Milli-Q water purifying system ($18 \text{ M}\Omega \text{ cm}^{-3}$) was used for all experiments. 0.1 M phosphate buffer solution (PBS) was prepared from NaH_2PO_4 and Na_2HPO_4 . All the electrochemical experiments were performed at room temperature ($21 \pm 0.5^\circ\text{C}$), expect particular introductions.

2.2. Synthesis of GOM

GO was prepared from natural graphite (12500 mesh) as we reported before.^{32, 33} In a typical synthesis, 400 mg GO was dispersed in ethanol (200 mL) by ultrasonic treatment for 30 min. Then 2.0 g aniline was slowly added into the GO suspension with stirring vigorously for about 1 h. The polymerization was then initiated by the dropwise addition of 125 mL 0.24 M KMnO_4 aqueous solution and the mixture maintained at room temperature for one hour.

Afterward the precipitate was collected by centrifugation at 8000 rpm for 15 min and washing repeatedly with distilled water. The as-prepared composite was signed as GOM.

2.3 Synthesis of RGOM

The further synthesis of RGOM products were carried out by alkaline treatment with hot NaOH aqueous under different conditions.

Typically, GOM was re-dispersed uniformly into NaOH aqueous (4 M or 8 M) with stirring. Subsequently, the mixed solution was treated by traditional stirring at 90 °C or hydrothermal heating at 90 and or 120 °C. After 5 h treatment, all products were centrifuged and washed several times, finally dried at 60 °C overnight under vacuum.

The different concentrations of NaOH and heating methods were listed in Table 1, and the resulting composites under different experiments were accordingly named as RGOM1~RGOM5, respectively.

Table 1 The list of different experiments

Reaction ^a	Sample ^b	NaOH (M) ^c	Temperature (°C) ^d	Method ^e
1	RGOM1	4	90	stirring
2	RGOM2	8	90	stirring
3	RGOM3	4	90	hydrothermal
4	RGOM4	4	120	hydrothermal
5	RGOM5	8	120	hydrothermal

^a The number of reactions; ^b The name of reaction products; ^{c, d, e}

Different concentration of reducing agent, temperature and method of each reaction, respectively.

2.4. General characterization

Powder X-ray diffraction (XRD) analyses were performed on a Bruker D8 Advance diffractometer with Cu K α radiation ($\lambda = 1.5406$ Å). The diffraction data were recorded for 2θ angles between 10° and 80°. The Raman spectra were recorded from 100 to 4000 cm⁻¹

on a Renishaw Invia Raman Microprobe using a 514.5 nm argon ion laser. The FTIR measurements of different samples were performed using a Fourier transform infrared (FTIR) spectrometer (Perkin-Elmer Spectrum one) in the wave number range from 4000 to 500 cm⁻¹, the KBr disk method was employed. Morphological analyses of the samples were carried out on a JEOL JEM-2100 TEM. Energy dispersive X-ray Spectrometer (EDS) measurements were performed on a JEOL JSM-6380LV Scanning Electron Microscope. For TEM measurement, the samples were re-dispersed in ethanol by ultrasonication and dropped on carbon-copper grids. The other analyses were tested by using powder as obtained.

2.5. Electrochemical characterization

For electrochemical measurements, the composite electrodes as working electrode were prepared according to the following steps: the as-prepared composites, acetylene black, and polytetrafluoroethylene (1%wt) with mass ratio 85: 10: 5 were mixed to form slurry, successively pressed onto a nickel foam (10 MPa), and dried under vacuum at 60 °C for 24 h. All electrochemical experiments were carried out in 1 M Na₂SO₄ using a three electrode system, in which platinum foils and saturated calomel electrode (SCE) were used as counter electrode and reference electrode, respectively. Cyclic voltammetry (CV) and electrochemical impedance spectroscopy (EIS) measurements were performed with a CHI760C workstation. The CV scan rates were in the range from 1 mV s⁻¹ to 100 mV s⁻¹ at the potential of 0 to 1.0 V. EIS tests were carried out in the frequency range 10⁻³ to 10⁵ Hz at open circuit potential with an AC perturbation of 5 mV. Galvanostatic charge-discharge testing was done from 0 to 1 V in 1 M Na₂SO₄, using a Land Battery workstation at 22 °C.

3. Results and discussion

3.1. Characterization of ternary composites

The typical FTIR spectrum was tested to identify the structures of the as-prepared GOM ternary composites. As shown in Fig. 1a, in the 1600-800 cm^{-1} region the characteristic peaks assigned to PANI, are corresponding to the aromatic ring, the N-H deformation and the C=N stretching vibration modes. The bands near 1580 and 1420 cm^{-1} are respectively related to the quinonoid (Q) and benzenoid (B) units

of PANI chains. Another main vibration band at 1338 cm^{-1} can be assigned to the C-N stretching mode of the aromatic amine structure, together with the vibration of C-O-C of GO. The two peaks at 1181 and 1061 cm^{-1} are assigned to the stretching of C-H in-plane and C-H out-of-plane bending on 1, 4-ring of polyaniline. Besides, the peaks below the 680 cm^{-1} can be ascribed to Mn-O stretching vibrations.³⁴

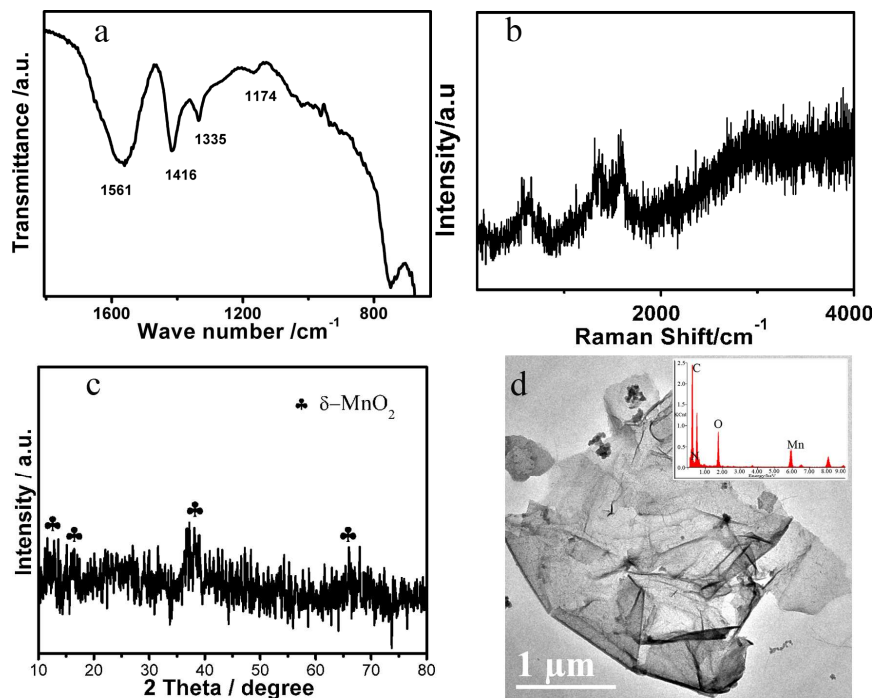


Fig. 1 FTIR spectrum (a), Raman spectrum (b), XRD pattern (c), TEM image (d) of GOM composite and in the inset of (d) is EDS spectrum.

In order to further characterize the ternary composite, Raman spectrum and the typical XRD pattern together give an indication of the structure of the GOM composite, and the TEM image clearly shows the morphology of GOM. The results are shown in Fig. 1.

From the Raman spectrum of GOM in Fig. 1b, the most intensive peaks around 1370 and 1586 cm^{-1} positions are corresponding to the D and G peaks of GO which overlapping with the peaks of the Q and B units in PANI. The existence of D peak proves that the GO flakes have significant defects.³⁵ Moreover, the Raman

characteristic peak of manganese oxide is obviously observed at about 651 cm^{-1} .³⁶

The XRD diffraction pattern is shown in Fig. 1c to confirm the crystalline structure of GOM. The peaks at 12.8, 17.8, 37.4 and 66.54° are associated with δ -MnO₂ (JCPDS card NO.44-1386, space group: I2/m, $a_0 = 9.943 \text{ \AA}$, $b_0 = 2.866 \text{ \AA}$, $c_0 = 9.709 \text{ \AA}$), and the first three peaks are respectively corresponding to the (101), (200) and (211) planes of δ -MnO₂.³⁷ A wide peak at 20-30° also

can be observed, which may be assigned to the diffraction peaks of PANI.

In the Fig. 1d, the representative TEM of GOM exhibits that GO sheets have rough surface which is attributed to the PANI and MnO₂ nanoparticles depositing on the surface of GO sheets. It indicates that the GO sheets act as support materials for loading the PANI and MnO₂ nanoparticles. Meanwhile, on the basis of the EDS spectrum of GOM in the inset of Fig. 1d, it displays the existence of C, O, Mn and N elements and the atomic percentage is estimated to be 65.01%, 28.08%, 5.21%, and 3.70%, respectively.

With the structure and morphology characterizations, it indicates that the GOM nanostructure is composed of PANI and MnO₂ nanoparticles randomly growing on the well-spread GO sheets.

After hot treatment in alkaline solution under different methods, various RGOM composites were acquired from the second step as described in Scheme 1. Different parameter changes of NaOH concentration, temperature, and heating method were carried out. The structure and morphology were characterized by FTIR, Raman and TEM. In addition, the variations in the crystalline state of RGOM samples were analysed by a careful XRD study.

Compared with GOM, different RGOM samples show some changes in chemical structures which can be reflected from FTIR (Fig. 2). The FTIR spectra of RGOM1 and RGOM2 show the similar characteristic peaks implying that the backbone structure of PANI was not changed much at 90 °C under stirring in alkaline solution with either low concentration (4 M) or high concentration (8 M). The slight left-shift in FTIR spectra of RGOM1 and RGOM2 composites illustrates the enhanced conjugative effect maintaining between PANI and RGO by π - π interaction due to the recovered conjugative plane of graphene.

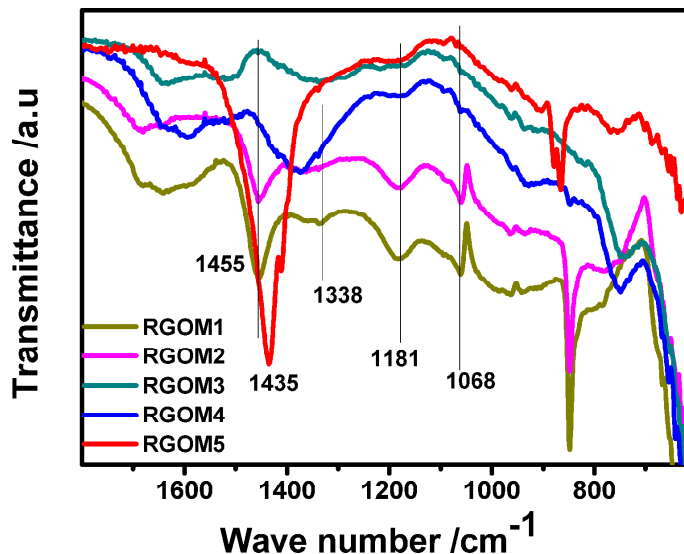


Fig. 2 FTIR spectra of RGOM1, RGOM2, RGOM3, RGOM4 and RGOM5.

However, after hydrothermal treatment, the FTIR spectra of RGOM3, RGOM4 and RGOM5 have great changes in some peaks compared with RGOM1 and RGOM2. From the Fig. 2, the FTIR characteristic peaks of PANI such as the peaks at 1561 and 1335 cm⁻¹ become either broader or weaker in RGOM3. The changes of FTIR spectra between RGOM1 and RGOM3 reflect that the hydrothermal technique has a great influence on the structure of RGOM. Compared the FTIR spectra between RGOM3 and RGOM4 which obtained respectively at 90 and 120 °C under the same method of hydrothermal condition, the obvious shifts of some peaks of RGOM4 can be observed. Besides, in the RGOM4 sample, some characteristic bands of the PANI backbone vanish or shift indicating the structure changes of PANI. It is explained that the hydrothermal temperature also plays an important role in the structure control of RGOM.

Notably, a contrast between RGOM4 and RGOM5 is found that there are the greatest changes of FTIR spectra in the range of 1200-1500 cm⁻¹ which covers the typical vibration peaks of PANI and reduced graphene oxide. It means that, under the hydrothermal

condition of 120 °C, the higher concentration of alkali can influence the structure of RGOM dramatically.

The structure changes of the nanocomposites could be also illustrated by Raman. Fig. 3a shows the Raman characteristic peaks of manganese oxide and RGO in RGOM1, RGOM2 and RGOM3 prepared at 90 °C. It is found that the shape and relative intensity of the D and G peaks among three RGOM samples occur change due to their different deoxygenating degrees of GO in hot strong alkaline solution, which could lead to the disorder of graphene.

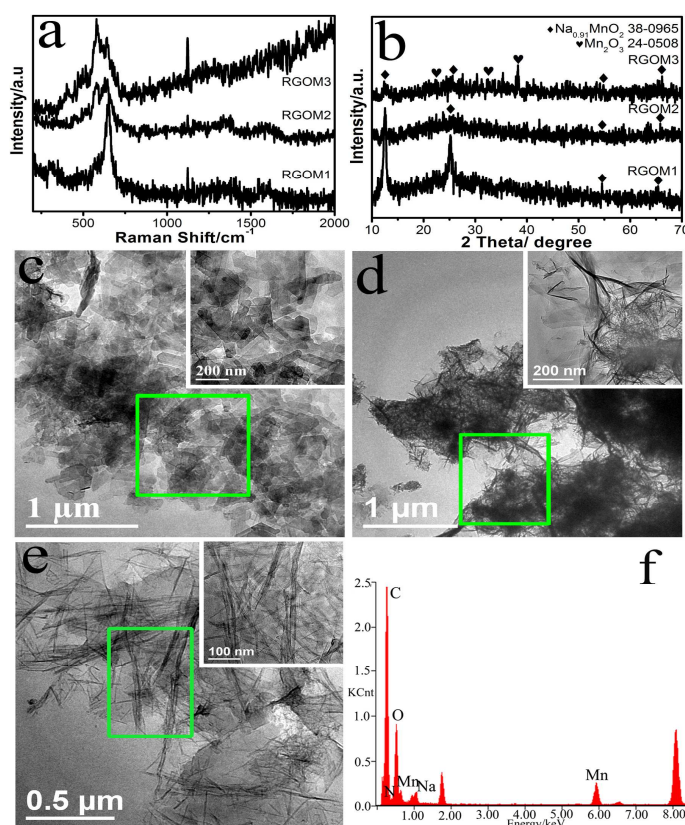


Fig. 3 Raman spectra (a); XRD (b); TEM images of RGOM1 (c), RGOM2 (d) and RGOM3 (e); EDS spectrum of RGOM1 (f).

XRD patterns were further used to study the influence of different conditions on the crystalline states of the final products of RGOM. As shown in Fig. 3b, the XRD diffraction patterns of RGOM1 and

RGOM2 obtained at 90 °C under stirring shows typical peaks at 12.5, 25.0, 54.8, and 65.5° indexing to the Na_{0.91}MnO₂ phase (JCPDS card no. 38-0965, orthorhombic, a₀ = 4.0519 Å, b₀ = 7.1195 Å, c₀ = 2.9837 Å). And the Na/Mn which evaluated by EDS is about 0.91 in accordance with the atom ratio of Na_{0.91}MnO₂ (Fig. 3f). The diffraction peaks at 12.5 and 25.0° associate with the (101) and (110) planes of a dehydrated Na-birnessite phase.³⁸ But the difference is that the XRD pattern of RGOM1 shows stronger peaks than RGOM2. It means the NaOH concentration under stirring at 90 °C can influence the crystalline state of Na_{0.91}MnO₂.

While, for the composite of RGOM3 obtained at 90 °C by hydrothermal method, its XRD diffraction pattern contains two crystalline states. In addition to Na_{0.91}MnO₂, another crystalline phase in the RGOM3 sample is β-Mn₂O₃ (JCPDS card no. 24-0508, orthorhombic, space group: Pcab, a₀ = 9.4158 Å, b₀ = 9.4238 Å, c₀ = 9.4046 Å, 2θ = 23.7, 32.4, 37.9°). The peaks appeared at 2θ = 23.7, 32.4° are corresponding to the (211) and (222) planes of β-Mn₂O₃.³⁹ But these peaks are weak suggesting the poor crystalline state of β-Mn₂O₃ in the RGOM3 composite. The existence of β-Mn₂O₃ in RGOM3 with comparison of RGOM1 implies that the redox reaction occurred during the hydrothermal process. It further indicates that, at the same temperature, the hydrothermal technique can facilitate the reduction of manganese oxide in the composite.

The TEM images of RGOM1, RGOM2 and RGOM3 are illustrated in Fig. 3(c, d and e). After reduced at 90 °C with stirring, the MnO₂ particles of GOM (Fig. 1c) converted to rod-like or short fiber-like Na_{0.91}MnO₂ on RGO sheets to form RGOM1 or RGOM2. Moreover, it is observed that RGOM1 contains big regular rods, which is well agreement with the strong XRD diffraction peaks of Na_{0.91}MnO₂.

However, RGOM2, obtained in 8 M NaOH, consists of the longer and thinner fibers of $\text{Na}_{0.91}\text{MnO}_2$, suggesting that high alkaline content may be beneficial for growing one-dimensional (1-D) long chain. While, as we can see in Fig. 3b, RGOM3 obtained at 90 °C by hydrothermal treatment shows more long fibers on and out of RGO sheets which consists of $\text{Na}_{0.91}\text{MnO}_2$ and Mn_2O_3 demonstrated by XRD analysis. And all the long fibers disperse loosely in the composite. The EDS spectrum of RGOM1 is shown in Fig. 3f. The relative content of oxygen reduces greatly with comparison of that of GOM (Fig. 1d). It proves the successful reduction of GO in the RGOM1 composite. The presence of low levels of oxygen may be derived from manganese oxide. And the N/Mn ratio of RGOM1 is estimated as 2.68/3.78 (~0.71, the same as that of GOM). It reveals that PANI was still kept in this reduction process.

All the results of above three composites indicate that the high NaOH concentration and hydrothermal condition greatly influence the morphologies of the RGOM and the crystalline transition of manganese oxide. In order to provide the clear insight into the mechanism for crystalline transition of manganese oxide, the reaction temperature and concentration of NaOH under hydrothermal treatment were investigated. The Raman, XRD and TEM results of the final products of RGOM4 and RGOM5 are shown in Fig.4 (a, b, c, and d).

Compared to RGOM1-RGOM3, the Raman peaks of RGOM4 and RGOM5 at about 651 cm^{-1} become narrow, it is probably due to the increasing crystalline of manganese oxide nanofibers (Fig. 4a). And two smaller peaks of RGOM5 sample can be observed at about 310 and 350 cm^{-1} ascribed to Mn_3O_4 which are in good agreement with the literature data. And the D and G peaks of graphene also weaken

even disappear, indicating that the structures of graphene and PANI might be changed.

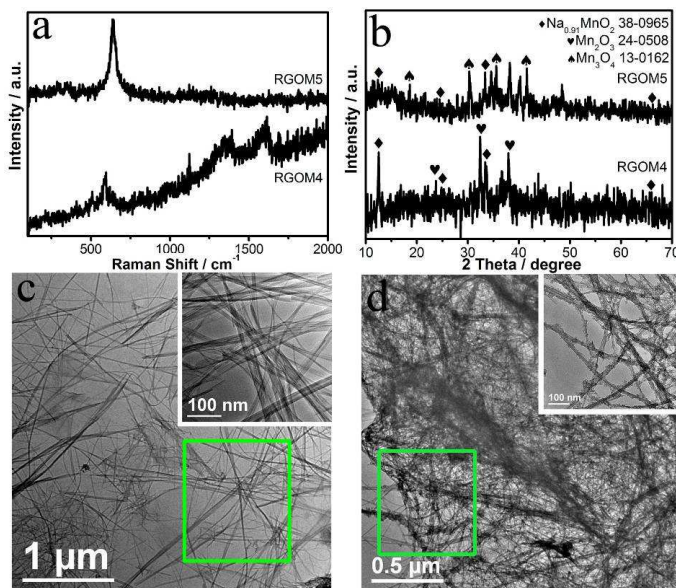


Fig. 4 Raman spectra (a), XRD (b) and TEM images of RGOM4 (c) and RGOM5 (d).

As shown in Fig. 4b, the XRD diffraction pattern of RGOM4 prepared in 4 M NaOH at 120 °C contains the similar peaks as those of RGOM3 obtained in 4 M NaOH at 90 °C, which shows the typical peaks at 12.5 , 25.0° and 23.7 , 32.4 , 37.9° matching well with the standard values of $\text{Na}_{0.91}\text{MnO}_2$ and $\beta\text{-Mn}_2\text{O}_3$, respectively. The difference is that the peak intensities of RGOM4 are higher than those of RGOM3 indicating the better crystalline feature of RGOM4 due to high temperature during hydrothermal process.

While for the RGOM5 prepared in 8 M NaOH at 120 °C, its XRD pattern not only shows the characteristic peaks of $\text{Na}_{0.91}\text{MnO}_2$, but also has the characteristic peaks at 18.6 , 30.3 , 35.3 and 41.6° which match well with Mn_3O_4 (JCPDS card no. 13-0162, cubic, space group: Fd-3m , $a_0 = 8.4195\text{ \AA}$). The strong peak appears at $2\theta = 35.3^\circ$ corresponding to (311) plane of Mn_3O_4 . Therefore, a new manganese oxide phase of Mn_3O_4 with lower valence appeared in

RGOM5 which was obtained in 8 M NaOH. It indicates that the higher concentration of NaOH under hydrothermal treatment promotes the reduction of MnO_2 at a greater degree, as well as the high temperature makes the reaction more fully.

The TEM image of RGOM4 (Fig. 4c) displays much super long fibers of manganese oxide with several micrometers in length and about 10 nm in diameters which grown on and out of RGO sheets. Some fibers are even converted into the tunnel structure (inset of Fig. 4c). Compared with that of RGOM3, much more and longer fibers of manganese oxides and the weakened RGO sheets were produced at 120 °C. The phenomenon further indicates that the high temperature under hydrothermal condition can promote the formation of its fiber-like nanostructure.

At the same temperature of 120 °C, RGOM5 prepared in 8 M NaOH demonstrates a rough and sheathed nanostructure with super long fibers covered by the irregular small sheets (Fig. 4d). Moreover, the original large carbon sheets in GOM (Fig. 2c) or RGOM4 (Fig. 4c) can't be observed any more. According to the changes of manganese oxide in XRD patterns, one can conclude that, under hydrothermal condition, manganese oxide were reduced to $\beta\text{-Mn}_2\text{O}_3$ or Mn_3O_4 by the reducing agent of carbon, and the large graphene sheets were simultaneously oxidized to small pieces.

The EDS pattern of RGOM5 (Fig. 5) shows that the relative content of oxygen greatly reduces compared with that of GOM (Fig. 2d), indicating the successful reduction of GO in the RGOM composites. Meanwhile, the N/Mn ratio of RGOM5 is found as 3.91/5.51 (~0.71), the same as those of GOM and RGOM1. It reveals that the component of PANI was also still kept in the final RGOM5 during the reduction process of hydrothermal treatment. Compared with that of RGOM1, the Na/Mn ratio of RGOM5

changed from 3.45/3.78 to 3.36/5.51, which indicates that a small amount of $\text{Na}_{0.91}\text{MnO}_2$ as an intermediate was reduced to the lower valence manganese oxide of Mn_3O_4 in the hydrothermal reduction process.

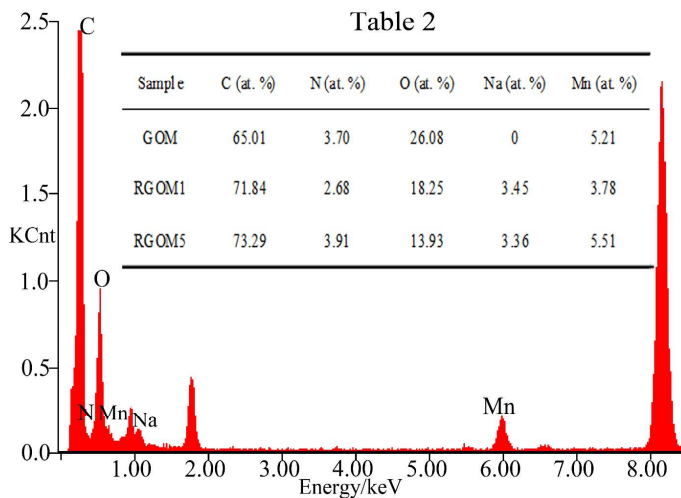
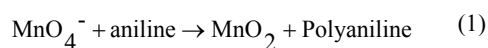


Fig. 5 EDS spectra of RGOM5 and the inset is the EDS data analysis table of GOM, RGOM1 and RGOM5.

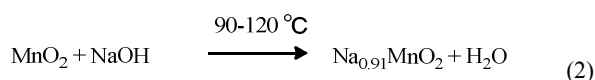
3.2 Growth mechanism and phase transformation of the composites

According to the above results and analysis, we propose a hypothesis about the reaction mechanism during the different synthetic processes. The mechanism of growth and varied morphologies of RGOM are illustrated in Scheme 1.

Briefly, in the first step reaction, KMnO_4 acted as an oxidant agent, and aniline served as a reducing agent. Aniline was oxidized and further polymerized to form the PANI chains, and aqueous KMnO_4 was converted to insoluble MnO_2 particles. Both PANI and MnO_2 particles simultaneously grew on the GO sheets as the support to produce the GOM composite. In this case, the nitrogen element in GOM composite can be only introduced by PANI. The reaction can be given by the equation (1) (Eq. 1):



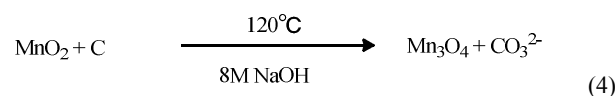
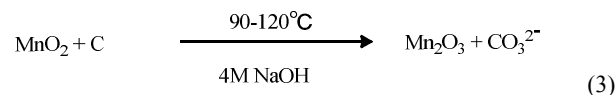
In above neutral reaction system, δ -MnO₂ was obtained which confirmed by XRD pattern. When the GOM sample was further treated in the hot NaOH solution, Na ions and H₂O with δ -MnO₂ could readily form Na⁺ hydrates (Na-typed birnessite) under magnetically stirring. Mn⁴⁺ ions in the manganese dioxide occurred a disproportionated reaction to Na_{0.91}MnO₂ as described in the following Eq. 2.^{38,40} And this hydrated forms can act as structure director for the fabrication of 1-D materials.⁴¹ Due to the mixed-valence manganese framework, it requires for a few cations (Na⁺) to balance the charge of Mn-O bands. On the basis of the guiding role of Na-typed birnessite, the small nanocrystalline of MnO₂ on the GO sheets as the nucleation site continuously grew into nanorods and nanofibers, even nanotubes. Moreover, the TEM images of RGOM1, RGOM2 (acquired under stirring conditions), RGOM4 and RGOM5 (under hydrothermal conditions) illustrate that the length of manganese oxide fibers increases with the rise of pH.



Besides the reaction (2), other different convention or transformation process also occurred in the hot-basic environment with different reaction conditions.

During the hot-alkaline treatment, GO could undergo quick deoxygenating as the previous report.⁴² And our experiment results identify that the content of oxygen in RGOM samples is greatly cut down, according to the data of EDS (Fig. 5). In the deoxygenating process, a number of defect sites were formed on graphene sheets. The carbon atoms of these sites had high activity to possibly reduce manganese oxide to low valence under hydrothermal condition.⁴³

In 4 M NaOH solution at 90 °C by a hydrothermal method, only a small amount of manganese oxide was slightly reduced to β -Mn₂O₃ phase (Eq. 3). That is why RGOM3 shows the mixed crystalline phases of Na_{0.91}MnO₂ and β -Mn₂O₃ confirmed by XRD. The relative high temperature and pressure environment of hydrothermal can devote quick kinetic reaction. Therefore, at 120 °C in 4 M NaOH, the more β -Mn₂O₃ was produced in RGOM4.



Under the more corrosive hydrothermal condition of 8M NaOH and 120 °C, the carbon sheets with defect sites could possess higher activity to convert manganese oxide to Mn₃O₄ with lower valence (Eq. 4). Meanwhile, the graphene oxide sheets have been probably cut into small pieces at its defect sites. Therefore, no large carbon sheets was clearly observed in the TEM image of RGOM5 (Fig. 4d), and only long manganese oxide fibers were covered by broken sheets. The manganese oxide fibers are mainly consisted of Mn₃O₄ and less Na_{0.91}MnO₂. It results in a rough nanostructure consisted of broken graphene pieces-PANI covering metal oxide fibers. Such a rough and sheathed nanostructure might enlarge the special surface area and then contribute to the electrochemical properties of RGOM5.

3.3 Electrochemical testing of the as-prepared composites

In order to explore the electrochemical property of as-synthesized GOM and RGOM nanocomposites, electrochemical measurements including CV, EIS and galvanostatic charge/discharge techniques with a three-electrode system were applied.

The CV measurement was carried out in 1 M Na₂SO₄ solution with the potential windows from 0 to 1 V. As shown in Fig. 6a, all the CV curves of GOM, RGOM1, RGOM2, RGOM3, RGOM4 and RGOM5 are near rectangular shape indicating these composites can be used as capacitive materials, and those of GOM and RGOM5 possess the biggest rectangular area than others. Meanwhile, a pair of redox peaks at 0.34 / 0.69 V in CV curves of the other four composites can be obviously observed assigning to the redox peaks of manganese oxide. The electrochemical behaviours combine with the double layer capacitance of electrode materials and pseudocapacitance from the redox reaction of manganese oxide and PANI, although the redox peaks of PANI are not obvious.

According to the absolute area of the CV curve, the specific capacitance (C , F·g⁻¹) can be calculated according to the following equation:

$$C = \frac{\int IdV}{vmV} \quad (5)$$

Where C is the specific capacitance of electroactive materials, m is the mass of the electroactive materials in the electrodes (g), I is the response current (A), V is the potential (V), v is the potential scan rate (V s⁻¹). As shown in Fig 6a, it can be calculated that the specific capacitance C are 324 F·g⁻¹ for GOM, 255 F·g⁻¹ for RGOM1, 334 F·g⁻¹ for RGOM2, 242 F·g⁻¹ for RGOM3, 230 F·g⁻¹ for RGOM4 and 344 F·g⁻¹ for RGOM5. The C values of RGOM2 and RGOM5 are higher than GOM, especially much higher than RGOM1, RGOM3 and RGOM4. The increased electrochemical performance might result from the high reduction degree of RGO under higher concentration of NaOH and the resulting nanostructure of the materials. The partial recovery of graphene structure and the crystal transition of manganese oxide are also benefit for the enhancement of electrochemical properties. While

the C values of RGOM1, RGOM3 and RGOM4 are lower than that of GOM, it can be explained that the low alkaline concentration is unfavourable for the sufficient reduction of GO.

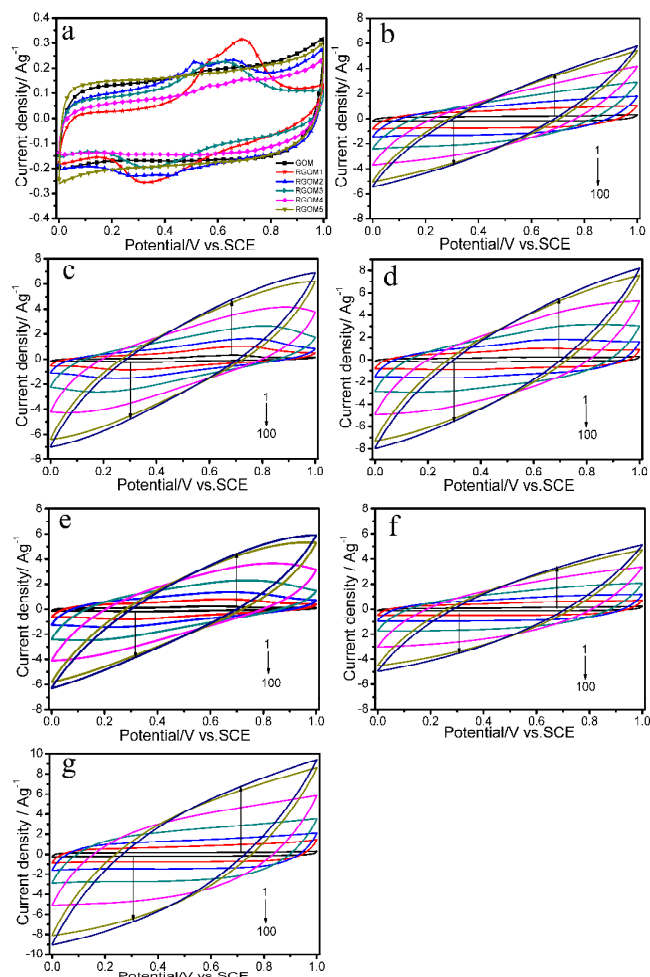


Fig. 6 (a) CVs at the scan rate of 1 mV s⁻¹ and (b-g) CVs at different scan rates of GOM, RGOM1, RGOM2, RGOM3, RGOM4 and RGOM5, respectively.

In order to get more information about the potential of RGO/manganese oxide/PANI ternary composites as electrode materials for a supercapacitor, the galvanostatic charge/discharge measurements were carried out in 1 M Na₂SO₄ at the current density of 500 mA·g⁻¹. As shown in Fig. 7a, all the curves exhibited an equilateral triangle shape suggesting the good reversibility during the charging and discharging process.

Moreover, the potential variations deviated from ideal linear line indicating that C value of the electrode materials is composed of the double layer capacitance and pseudocapacitance. It is attributed to the different components in the composites and their synergetic

effect among manganese oxide, RGO and PANI. At the same time, the small or even negligible voltage drop indicates that the ternary composite electrodes show low internal resistance.

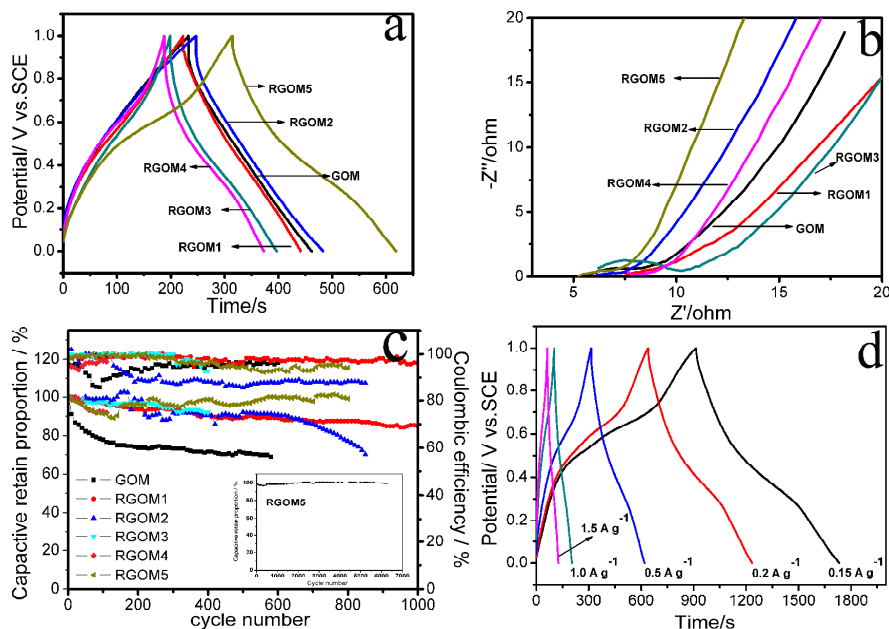


Fig. 7 (a) Charge-discharge curves got in 1 M Na₂SO₄ at the current density of 500 mA g⁻¹; (b) The Nyquist plots; (c) Coulombic efficiencies and capacitive retention proportions at 500 mA g⁻¹ of GOM, RGOM1, RGOM2, RGOM3, RGOM4 and RGOM5, respectively, the inset shows the cycling stability of RGOM5 after 6000 cycles at 1 A g⁻¹; (d) Charge-discharge curves of RGOM5 at different current densities.

EIS tests were used to further evaluate the electrochemical behaviours. The ideal Nyquist impedance plot includes a small semicircle indicating low interfacial charge-transfer resistance (R_{ct}) at higher frequencies, whereas vertical linear section corresponding to an ideal capacitor at lower frequencies. Fig. 7b displays the Nyquist plots of the various electrode materials which tested at the frequency range from 10⁻³ to 10⁵ Hz in 1 M Na₂SO₄ solution. A smaller semicircle can be observed for RGOM1, RGOM2, RGOM4 and RGOM5 than GOM, while that of RGOM3 exhibits the biggest semicircle. The semicircle is usually expected to be on the behalf of capacitance in parallel with the ionic charge-transfer resistance. It is related to the interface process between electrode material and

electrolyte. As shown in Fig. 7b, the values of R_{ct} for RGOM2 and RGOM5 are relatively smaller than the others due to the high conductivity of RGO obtained in 8 M NaOH. Furthermore, at the low frequency, the lines of RGOM2 and RGOM5 exhibit nearly close to 90° than the others. It shows better capacitance behaviour in consequence of the synergistic effect between RGO, PANI and manganese oxide. The results of EIS indicate that RGOM2 and RGOM5 possess the lower charge transfer resistance and better capacitive behaviours compared with GOM, RGOM1, RGOM3, and RGOM4, which is consistent with the CV tests. The advantages of RGOM2 and RGOM5 than other four prepared composites were clearly demonstrated.

More interestingly, the cycling stability of ternary composites modified electrodes was also investigated by galvanostatic charge/discharge measurement in 1 M Na₂SO₄ solution between 0 to 1 V. Fig. 7c shows that the *C* retention of the composite is about 69% after 580 cycles for GOM, 85% after 1000 cycles for RGOM2 and nearly 100% after 800 cycles for RGOM5, respectively. However, the *C* retentions of RGOM1, RGOM3 and RGOM4 are not stable. Even the *C* retention of the RGOM5 retains nearly 100% after 6000 cycles (the inset of Fig. 7c), suggesting that good cycling stability of RGOM5, while the long cycles led to the nanostructure change or fracture of GOM, RGOM1, RGOM2, RGOM3 and RGOM4. The excellent stability of RGOM5 may arise from its well-designed manganese oxide nanofibers sheathed with RGO and PANI. As shown in the Fig. 7d, the galvanostatic charge/discharge of RGOM5 with varied current densities indicates that it possesses well rate performance. Such a nanostructure RGOM5 with high electrochemical performance has a promise for electrode materials in the application of supercapacitors.

4. Conclusions

We successfully synthesized a ternary GO / MnO₂ / PANI nanocomposite by a one-step method at room temperature using KMnO₄ as the oxidant and initiating agent for the polymerization of aniline. The reduced graphene oxide / manganese oxide / PANI nanocomposites (RGOM1 - RGOM5) with various morphologies and different manganese oxides were fabricated via the hot-alkaline treatment of GO / MnO₂ / PANI under stirring or hydrothermal conditions. It is found that the reaction temperature and the concentration of alkali play important roles in the formation of nanofiber-like structure and the crystalline transformation of manganese oxide during the reaction process. The higher temperature and higher concentration of NaOH in the hydrothermal

process can facilitate the redox reaction between carbon and manganese oxide. The RGOM5 nanocomposite with super long fibers covered by thin carbon sheets, prepared using 8 M NaOH at 120 °C via a hydrothermal method, exhibits the highest specific capacitance of 344 F·g⁻¹ and good cycle performance with nearly 100 % after 6000 cycles. The excellence performances of specific capacitance, good rate capacity and cycle stability contribute to the rough and sheathed nanofiber-like structure which is able to increase large special area and realize fast electron transport. The ternary composites with the advantages of synergistic effects among RGO, Mn₃O₄ and PANI components could be promising electrode material for supercapacitors as well as for other application. The ternary composites of RGOM with rough and sheathed nanofiber-like structure could be promising electrode material for supercapacitors as well as for other application.

Acknowledgements

The work was supported by the National Natural Science Foundation of China (No. 21103092), Program for NCET-12-0629, the National High Technology Research and Development Program of China (863 Program, No. 2013AA050905), the Ph.D. Programs Foundation of Ministry of Education of China (no. 20133219110018), the Fundamental Research Funds for the Central Universities (No. 30920130111003), Qing Lan Project and Six Major Talent Summit (XNY-011), the Science and Technology Support Plan and PAPD of Jiangsu Province, China (No. BE2011835 and BE2013126).

Notes and references

^a School of Chemical Engineering, Key Laboratory for Soft Chemistry and Functional Materials, Ministry of Education, Nanjing University of Science and Technology, Nanjing, 210094, China. Tel.: +86-25-84315943; Fax: +86-25-84315190; E-mail: qinglihao@njjust.edu.cn; haoqingli@yahoo.com (Q. Hao)

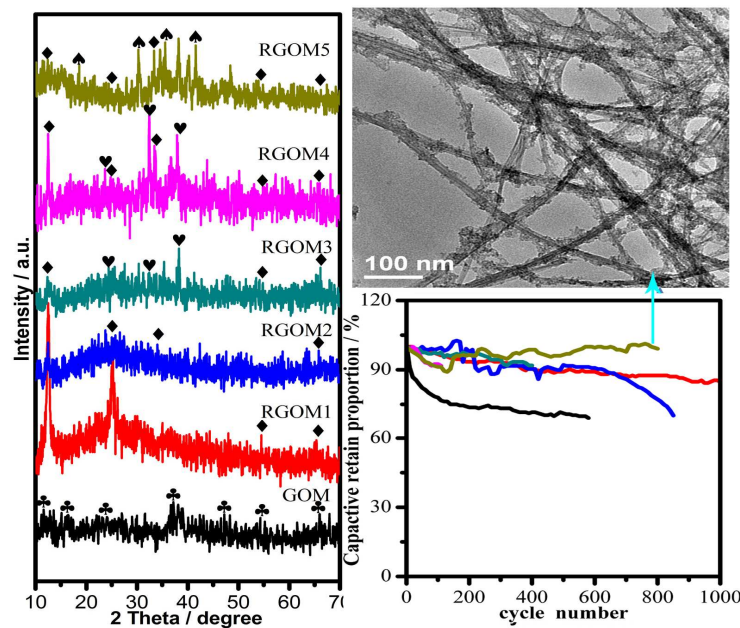
1. H. Y. Lee and J. B. Goodenough, *Journal of Solid State Chemistry*, 1999, **144**, 220-223.
2. R. Ko, *Electrochim. Acta*, 2000, **45**, 2483.
3. P. Simon and Y. Gogotsi, *Nat Mater*, 2008, **7**, 845-854.
4. B. Mendoza-Sánchez, B. Rasche, V. Nicolosi and P. S. Grant, *Carbon*, 2013, **52**, 337-346.
5. J. R. Miller, R. Outlaw and B. Holloway, *Science*, 2010, **329**, 1637-1639.
6. D. Qu, *Journal of Power Sources*, 2002, **109**, 403-411.
7. C. Tan, K. Tan, Y. Ong, A. Mohamed, S. Zein and S. Tan, *Environmental Chemistry Letters*, 2012, **10**, 265-273.
8. G. Zhang, J. Zheng, R. Liang, C. Zhang, B. Wang, M. Au, M. Hendrickson and E. Plichta, *Journal of The Electrochemical Society*, 2011, **158**, A822-A827.
9. E. Jacques, M. H. Kjell, D. Zenkert, G. Lindbergh, M. Behm and M. Willgert, *Composites Science and Technology*, 2012, **72**, 792-798.
10. Q. Lu, Q. Zhao, H. Zhang, J. Li, X. Wang and F. Wang, *ACS Macro Letters*, 2013, **2**, 92-95.
11. J. Ma, Y. Liu, Z. Hu and Z. Xu, *Ionics*, 2013, 1-9.
12. T.-S. Hyun, H. L. Tuller, D.-Y. Youn, H.-G. Kim and I.-D. Kim, *J. Mater. Chem.*, 2010, **20**, 9172-9179.
13. M. T. Brumbach, T. M. Alam, P. G. Kotula, B. B. McKenzie and B. C. Bunker, *ACS Applied Materials & Interfaces*, 2010, **2**, 778-787.
14. C. Xu, F. Kang, B. Li and H. Du, *Journal of materials research*, 2010, **25**, 1421-1432.
15. Z.-S. Wu, W. Ren, D.-W. Wang, F. Li, B. Liu and H.-M. Cheng, *Acs Nano*, 2010, **4**, 5835-5842.
16. J. R. Lake, A. Cheng, S. Selverston, Z. Tanaka, J. Koehne, M. Meyyappan and B. Chen, *Journal of Vacuum Science & Technology B: Microelectronics and Nanometer Structures*, 2012, **30**, 03D118-103D118-116.
17. D.-W. Wang, F. Li, J. Zhao, W. Ren, Z.-G. Chen, J. Tan, Z.-S. Wu, I. Gentle, G. Q. Lu and H.-M. Cheng, *Acs Nano*, 2009, **3**, 1745-1752.
18. W. Wei, X. Cui, W. Chen and D. G. Ivey, *Chemical Society Reviews*, 2011, **40**, 1697-1721.
19. T. Brousse, M. Toupin, R. Dugas, L. Athouël, O. Crosnier and D. Bélanger, *Journal of The Electrochemical Society*, 2006, **153**, A2171-A2180.
20. O. Ghodbane, J.-L. Pascal and F. Favier, *ACS Applied Materials & Interfaces*, 2009, **1**, 1130-1139.
21. S. Devaraj and N. Munichandraiah, *Journal of The Electrochemical Society*, 2007, **154**, A80-A88.
22. T. Nathan, M. Cloke and S. Prabaharan, *Journal of Nanomaterials*, 2008, **2008**, 81.
23. Z.-Y. Yuan, Z. Zhang, G. Du, T.-Z. Ren and B.-L. Su, *Chemical physics letters*, 2003, **378**, 349-353.
24. S.-B. Ma, K.-Y. Ahn, E.-S. Lee, K.-H. Oh and K.-B. Kim, *Carbon*, 2007, **45**, 375-382.
25. Y. Wang, Z. Shi, Y. Huang, Y. Ma, C. Wang, M. Chen and Y. Chen, *The Journal of Physical Chemistry C*, 2009, **113**, 13103-13107.
26. C. Selvaraj, S. Kumar, A. Raju and N. Munichandraiah, *Journal of Applicable Chemistry*, 2012, **1**, 272-287.
27. R. Liu and S. B. Lee, *Journal of the American Chemical Society*, 2008, **130**, 2942-2943.
28. S.-L. Chou, J.-Z. Wang, S.-Y. Chew, H.-K. Liu and S.-X. Dou, *Electrochemistry Communications*, 2008, **10**, 1724-1727.
29. F. Meng, X. Yan, Y. Zhu and P. Si, *Nanoscale research letters*, 2013, **8**, 1-8.
30. C. X. Guo, M. Wang, T. Chen, X. W. Lou and C. M. Li, *Advanced Energy Materials*, 2011, **1**, 736-741.
31. G. Wang, Q. Tang, H. Bao, X. Li and G. Wang, *Journal of Power Sources*, 2013.
32. Q. Hao, H. Wang, X. Yang, L. Lu and X. Wang, *Nano Research*, 2010, **4**, 323-333.
33. X. Xia, Q. Hao, W. Lei, W. Wang, D. Sun and X. Wang, *Journal of Materials Chemistry*, 2012, **22**, 16844.
34. D. P. Dubal, D. S. Dhawale, R. R. Salunkhe, S. M. Pawar and C. D. Lokhande, *Applied Surface Science*, 2010, **256**, 4411-4416.
35. A. Ferrari, J. Meyer, V. Scardaci, C. Casiraghi, M. Lazzeri, F. Mauri, S. Piscanec, D. Jiang, K. Novoselov and S. Roth, *Physical review letters*, 2006, **97**, 187401.
36. D. T. Zahn, *Physical Chemistry Chemical Physics*, 1999, **1**, 185-190.
37. H. Jiang, J. Ma and C. Li, *Journal of Materials Chemistry*, 2012, **22**, 16939-16942.
38. Y. Li and Y. Wu, *Nano Research*, 2009, **2**, 54-60.
39. K.-W. Park, *Journal of Materials Chemistry A*, 2014, **2**, 4292.
40. X. Tang, H. Li, Z.-H. Liu, Z. Yang and Z. Wang, *Journal of Power Sources*, 2011, **196**, 855-859.

Journal Name

41. X. F. Shen, Y. S. Ding, J. Liu, J. Cai, K. Laubernds, R. P. Zerger, A. Vasiliev, M. Aindow and S. L. Suib, *Advanced Materials*, 2005, **17**, 805-809.
42. X. Fan, W. Peng, Y. Li, X. Li, S. Wang, G. Zhang and F. Zhang, *Advanced Materials*, 2008, **20**, 4490-4493.
43. H. Xia, M. Lai and L. Lu, *Journal of Materials Chemistry*, 2010, **20**, 6896.

Graphical Abstract

Synthesis and Electrochemical Properties of Reduced Graphene Oxide / Manganese oxide / Polyaniline Composites



Graphene oxide/manganese oxide/polyaniline ternary composite and its reduced composites (RGOM) were synthesized. RGOM5 with rough and sheathed structure shows excellent electrochemical properties.